SIMULATION RESULTS OF A SMALL ANIMAL LIQUID XENON PET DETECTOR

Y. Grondin, M. Desvignes, L. Desbat, S. Mancini

Grenoble Universities
TIMC-IMAG, GIPSA-LAB DIS
38000 Grenoble France

M-L. Gallin-Martel, L. Gallin-Martel, O. Rossetto

Grenoble Universities
CNRS, LPSC laboratory
38000 Grenoble France

ABSTRACT

Monte Carlo simulations of a novel concept PET detector for small animal imaging are presented. The scintillation medium of the detector is liquid xenon whose characteristics in terms of detection rival with the common scintillator crystals. Moreover, the axial geometry of the detector enables depth of interaction measurement. A detector module has been built and an experimental test bench has been developed. Simulations of the test bench enabled to determine the methods to use for analysing the experimental data. Moreover, they indicate the spatial resolution in the axial direction and the energy resolution which can be expected from the detector. The results show an axial resolution of 2.87±0.12 mm and an energy resolution of 7.59±0.34%.

Index Terms— Positron Emission Tomography, scintillation detectors, Monte Carlo simulations.

1. INTRODUCTION

Small animal imaging is a challenging field of research since high sensitivity and resolution systems are needed to observe disease mechanisms or drugs functions. Positron Emission Tomography (PET) which enables to image molecular biological processes in vivo suits to this purpose. Several PET scanners designed for small animal imaging have been developed, such as MicroPET II [1]. Presently, most of these scanners based on radial crystal arrangements do not detect the depth of interaction (DoI) of photons in scintillators. The consequences are the degradation of the spatial resolutions because of the non negligible parallax error induced. Compared to clinical PET scanners, small animal PET imaging requires smaller crystals to improve spatial resolution. It results in the use of a scintillator medium having a high density and light yield. Furthermore, random coincidences increases in small animal PET scanners, which can be overcome by using a shorter coincidence window and therefore a short decay time crystal. We propose a novel concept of small animal dedicated PET scanner which is based on a liquid xenon (LXe) scintillator in an axial geometry enabling DoI measurement. PET scanner detectors radially or axially oriented and measuring DoI already exist for brain imaging [2, 3]. The originality of our work lies in the use of a material well known for its detection properties in astrophysics to medical imaging field. LXe is an excellent detecting medium for γ-rays due to his high atomic number and density. Its fast scintillation light yield is comparable to that of NaI. When compared to commonly used crystal (table 1), it appears that the decay time 3 to 30 ns is the shortest, the spread being due to the various scintillation modes of the Xe atom. Moreover, the liquid state of this medium enables different detector geometries to be easily tested.

Scintillator	Density ($g.cm^{-3}$)	Light Yield (UV/MeV)	Decay time (ns)
LXe	3.06	43000-78600	3-30
NaI	3.67	38000	230
BGO	7.13	9000	300
LSO	7.4	27000	40

Table 1. Comparison of physical properties of LXe and commonly used crystal

The proposed LXe PET scanner is composed of 16 modules as shown in figure 1 and 2. Each module presents a 2×2 cm^2 cross-section in the transversal plane of the camera. The whole scanner is immersed in a cryostat to keep the xenon liquid. The transversal field of view limited by the cryostat is 8 cm, whereas the axial field of view is 5 cm. Each module is filled of liquid xenon and is subdivided by 40 2×5 mm^2 MgF2-coated aluminium ultraviolet (UV) light guides. The scintillation UV photons propagate in the guide by specular reflections and are collected on both sides of each module by two Position Sensitive PhotoMultiplier Tubes (PSPMT). The (x, y) positions measured by the PSPMT determines which light guides have been fired. The light attenuation which depends on the guide reflectivity allows the axial coordinate z to be deduced from dynodes signals asymmetry. A prototype LXe module has been built. It has been simulated using the GATE [4] Monte Carlo code. In the first part of this paper, we describe the experimental set up that has been built to characterize our module in terms of energy, time and spatial resolution capabilities. This topic is discussed briefly : an upcoming

article will deal with the experimental aspect in details. Then, the Monte Carlo simulations principle of the test bench and the model of the z (axial) coordinate analytical calculation are reported. In the second part, the simulations results and the axial and energy resolutions of the detector are presented.

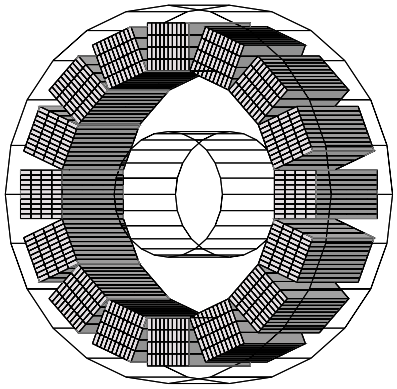

Fig. 1. 16 modules of detection in the cryostat

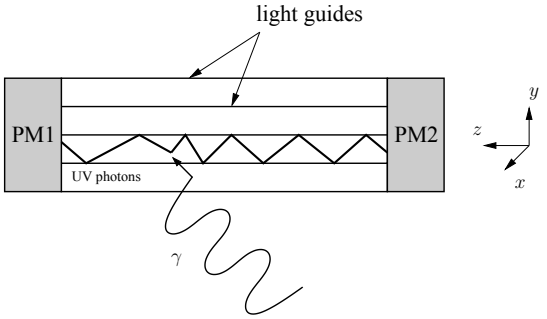

Fig. 2. A module of detection along the axial direction

2. MATERIALS AND METHODS

2.1. Experimental set up

An experimental test bench was built to allow the transversal localization of an interaction in the module, i.e. x and y measurements, but also to evaluate the axial localization (coordinate z) and the time resolution. As shown in figure 3, underneath the cryostat where the LXe cell is placed, a ^{22}Na source is mounted on a small carriage moving along the z

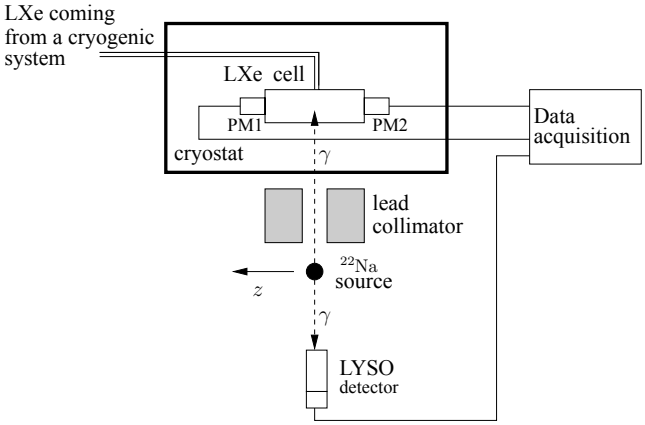

Fig. 3. Experimental set up scheme

axis. A LYSO crystal coupled to a photomultiplier tube completes the experimental set-up to make the coincidence signal. A registration of an interaction in the module is made only when the pair of γ photons hits the module and the LYSO. The lead blocks collimate the source emission in the direction orthogonal to the detection module. In this manner by moving the carriage, with a pitch of 5mm, the module is fired all along its axis and its response is measured for each source position.

2.2. Monte Carlo simulations principle

The test bench was simulated in GATE. The module was created as a square section box divided by 40 smaller boxes of rectangular section representing the light guides. The aluminium coats covering the light guides have not been simulated in GATE at the moment, their influence on the detection of the 511 keV gamma photons being considered negligible [5]. However, UV photon transport in the aluminium guides and detection resolution has been simulated with a custom MC code. The code is able to track individual scintillation photons from their emission point through the aluminium guide to the photodetectors, taking into account reflection as well as absorptions. However it does not include at the moment the photon detection process in the PSPMT and the readout electronics. The source was an hypothetical 511 keV gamma photons emitter placed below the detector. It was a sphere of 1 mm radius whose the activity was set to 1 million Bq. The lead blocks of the experiment were simulated. The LYSO was not simulated and therefore we have not simulated the detector time response. However, the LYSO was taken into account by simulating additional lead blocks such that, combined to the other blocks, the gamma photons are collimated through a square hole of the same area as the LYSO's sensitive surface. The physic processes implemented according the GEANT4 electromagnetic models package in GATE were the photoelectric effect and Compton scatter. Rayleigh

scatter was not simulated. The output data of the GATE simulations consisted in the collection of all interactions occurred in the detector and in the other simulated components of the set up. The most important features that are used for simulating the generation of the UV photons and therefore the detection in our MC code are the amount of deposited energy and the localization of the hits in the detector.

2.3. Light guide modelling

The DoI measurement in the context of axial geometry scanner consist in reconstructing the z position of the interaction point of the incident γ from the signals given by the two PSPMT's. Several models were presented by other groups working with this geometry. An approach introduced by the authors of [6] assumes that the amount of light collected at a crystal end decays exponentially with the axial z coordinate of the γ photon interaction point. With this model, the attenuation length λ_{ref} of the light guide can be introduced. If we assume that the intrinsic attenuation length λ_{int} of the LXe is much higher than λ_{ref}, the light attenuation in the detector can be described by the function:

$$I(z) = I_0 \exp\left(-\frac{z}{\lambda_{ref}}\right) \tag{1}$$

λ_{ref} depends on the light guide geometry and reflectivity, which is taken at 0.8 in our simulations. It also depends on a limit angle (LA) due to the fact that the PSPMT's are not immersed in the LXE and a thin gap is kept between the cell quartz window and the PSPMT entrance window. The UV photons encounter along their path different refraction indexes, 1.75, 1.58, 1.0 and finally 1.58 resulting in a LA of 38 degrees. The number of photoelectrons collected at each module end (N_L at the left, N_R at the right) is given by:

$$\begin{aligned} N_L(z) &= A\frac{N_0}{2}\exp\left(-\frac{\frac{l}{2}+z}{\lambda_{ref}}\right) \\ N_R(z) &= A\frac{N_0}{2}\exp\left(-\frac{\frac{l}{2}-z}{\lambda_{ref}}\right) \end{aligned} \tag{2}$$

where $z = 0$ corresponds to the center of the module, A a constant depending on LA and PMT quantum efficiency, N_0, the number of scintillation photons and l, the length of the detector.

3. RESULTS

3.1. Determination of the interaction point and z resolution

The first step to perform DoI measurement is to determine λ_{ref}. From equations (2), we derive:

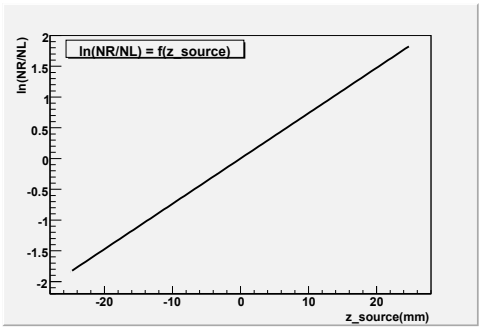

Fig. 4. Linear fit of $\ln\left(\frac{N_R}{N_L}\right)$ in function of z to determine λ_{ref}

$$\ln\left(\frac{N_R}{N_L}\right) = \frac{2z}{\lambda_{ref}} \tag{3}$$

A set of preliminary simulations is performed where the source is perfectly collimated and no Δz spread is introduced in the z coordinate interaction for a given source position. We determined λ_{ref} = 27 mm by the plot shown in figure 4. The linear behaviour confirms that the exponential model is satisfying at this stage of the analysis. Then, the reconstructed z, noted z_{rec}, is derived from equation (3):

$$z_{rec} = \frac{1}{2}\lambda_{ref}\ln\left(\frac{N_R}{N_L}\right) \tag{4}$$

Distribution of z_{rec} for a source located at z_{source} = -14.5 mm, is shown in figure 5.

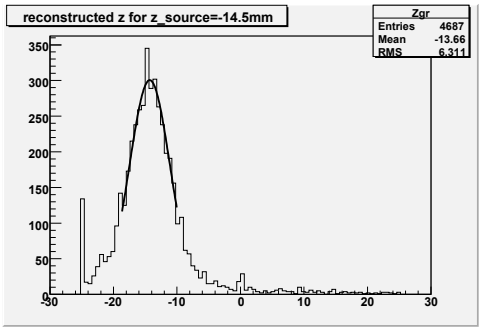

Fig. 5. A Gaussian fit of the reconstructed z position at z_{source} = -14.5 mm

A Gaussian fit of this distribution for different values of z_{source} provides the axial resolution of the module. Figure 6 shows the RMS value of the error on z_{rec} as a function of z_{source}. The module edges have not been taken into account because we observed a large deficit of UV photons due to the γ beam width. A mean axial resolution of 2.87±0.12 mm along the module is found.

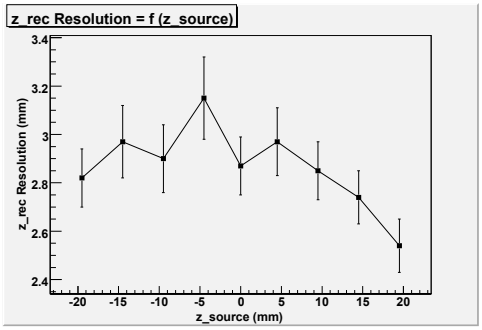

Fig. 6. z reconstructed resolution along the module

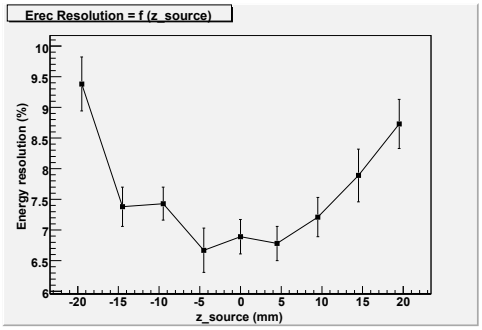

Fig. 8. Energy resolution along the module

3.2. Energy reconstruction and resolution

The energy resolution can be deduced from the total amount of photo-electrons collected for each z_{source}. Since the sum $N_L + N_R$ is not a constant along z axis, a correction factor $f_{cor}(z_{rec})$ has to be applied to get the reconstructed value of the energy E_{rec}:

$$E_{rec} = \frac{N_L + N_R}{f_{cor}(z_{rec})} \times 511\text{keV} \qquad (5)$$

$f_{cor}(z_{rec})$ is determined by using the same ideal preliminary simulations as for determining λ_{ref}. However, it turns out that the exponential model does not fit for determining E_{rec}. We therefore used a polynomial expression to calibrate $N_L + N_R$ in function of z_{rec} (determined by equation (4)) for each z_{source} position of the preliminary simulations. The spectrum of the sum $N_L + N_R$ obtained for z_{source} = -14.5 mm with a Gaussian fit is shown on figure 7. The same process is repeated for all source positions and the energy resolution for the whole module is obtained (figure 8). A mean energy resolution of 7.59±0.34% is found.

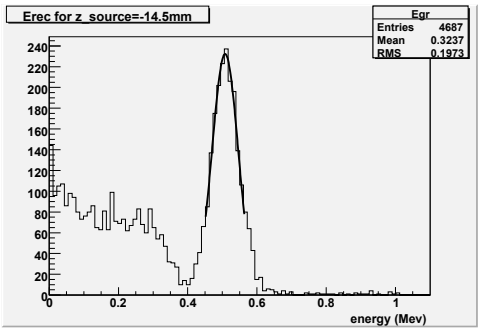

Fig. 7. A Gaussian fit of the reconstructed energy at z_{source} = -14.5 mm

4. CONCLUSION

The models that have been chosen to reconstruct the interaction point and the energy of the incident γ photon are satisfying. Specially, the exponential scheme which qualify the light propagation in the guides by a single λ_{ref} parameter enables to reconstruct the z coordinate. The experimental results have been therefore analyzed according to these methods and will be presented in another article. The simulated performances of the LXe detector show a mean axial resolution of 2.87±0.12 mm and a mean energy resolution of 7.59±0.34%. Time resolution has not been simulated for the moment. These results are promising and the simulation of the whole scanner is underway to quantify the performances on reconstructed images.

5. REFERENCES

[1] Y.C Tai et al, "Micropet 2:design, development and initial performance of an improved micropet scanner for small-animal imaging," *Phys. Med. Biol*, vol. 48, pp. 1519–1537, 2003.

[2] K. Wienhard et al, "The ecat hrrt: performance and first clinical application of the new high resolution research tomograph," *IEEE Trans. Nucl. Sci.*, vol. 49, pp. 104–110, 2002.

[3] A. Braem et al, "Feasibility of a novel design of high resolution parallax-free compton enhanced pet scanner dedicated to brain research," *Phys. Med. Biol*, vol. 49, pp. 2547–2562, 2004.

[4] S. Jan et al, "Gate: a simulation toolkit for pet and spect," *Phys. Med. Biol*, vol. 49, pp. 4543–4561, 2004.

[5] S.Jan, *Simulateur Monte Carlo et caméra à xénon liquide pour la Tomographie à Emission de Positons*, Ph.D. thesis, Université Joseph Fourier - Grenoble, 2002.

[6] A. Braem et al, "Scintillator studies for the hpd-pet concept," *Nucl. Instrum. Methods A*, vol. 571, pp. 419–424, 2007.